

# Ultracold bosons in lattices with binary disorder

K. V. Krutitsky,<sup>1</sup> M. Thorwart,<sup>2</sup> R. Egger,<sup>2</sup> and R. Graham<sup>1</sup>

<sup>1</sup>*Fachbereich Physik der Universität Duisburg-Essen, Campus Duisburg, Lotharstr. 1, 47048 Duisburg, Germany*

<sup>2</sup>*Institut für Theoretische Physik, Heinrich-Heine-Universität, D-40225 Düsseldorf, Germany*

(Dated: November 3, 2018)

Quantum phases of ultracold bosons with repulsive interactions in lattices in the presence of quenched disorder are investigated. The disorder is assumed to be caused by the interaction of the bosons with impurity atoms having a large effective mass. The system is described by the Bose-Hubbard Hamiltonian with random on-site energies which have a discrete binary probability distribution. The phase diagram at zero temperature is calculated using several methods like a strong-coupling expansion, an exact numerical diagonalization, and a Bose-Fermi mapping valid in the hard-core limit. It is shown that the Mott-insulator phase exists for any strength of disorder in contrast to the case of continuous probability distribution. We find that the compressibility of the Bose glass phase varies in a wide range and can be extremely low. Furthermore, we evaluate experimentally accessible quantities like the momentum distribution, the static and dynamic structure factors, and the density of excited states. The influence of finite temperature is discussed as well.

PACS numbers: 03.75.Lm, 03.75.Hh, 67.85.Hj

## I. INTRODUCTION

The remarkable experimental control over ultracold atomic gases in optical lattices acquired in recent years [1, 2, 3, 4, 5, 6] has opened up completely new lines of investigation in the field of strongly correlated quantum systems. One of these are quantum phase transitions (QPTs) of ultracold atoms in optical lattices. These fascinating phenomena are caused by the interplay of quantum tunneling, atomic interaction and disorder. In contrast to other condensed-matter systems where quantum phase transitions can also take place, optical lattices provide a unique possibility to *control* the disorder which can be created by several methods. Truly random potentials with continuous disorder distribution can be created using laser speckles [7, 8, 9, 10] which leads to random contributions to the tunneling amplitudes as well as on-site energy shifts. In addition to that, the atomic interaction energies can be made random [11], if the lattice loaded by cold atoms is placed near a wire inducing a spatially random magnetic field [12]. Disorder with discrete probability distribution can be created introducing a second atomic species strongly localized on random sites [13, 14, 15] which leads only to random shifts of the on-site energies. With the aid of incommensurate lattices one can make the tunneling amplitudes and the on-site energies quasi-random [16, 17, 18].

Until recently, studies of QPTs in cold atoms were dealing with continuous disorder distributions of different types. QPTs in the presence of disorder with discrete probability distribution were studied only for interacting electrons in binary alloys [19]. The role of this type of disorder in QPTs of cold bosons starts to become also a subject of research [20]. In the present work, we shall investigate QPTs of ultracold bosons in a lattice with disorder which is created by the interaction with impurity atoms localized at random lattice sites. The underlying theoretical model is the Bose-Hubbard Hamiltonian with random on-site energies according to a binary probability distribution. The problem was recently addressed in the work by Mering and Fleischhauer [20], who employed the DMRG-method to study the system. Our analysis will be based either

on an exact numerical diagonalization for sufficiently small systems or a Bose-Fermi mapping for the case of hard-core bosons in a one-dimensional lattice. These exact methods will be applied to obtain the phase diagram at zero temperature. Moreover, the role of finite temperature will be studied. In addition, we evaluate experimentally accessible quantities, such as the momentum distribution, the static and dynamic structure factors and the density of excited states.

The paper is organized as follows. In Sec. II, we describe the theoretical model of the Bose-Hubbard Hamiltonian with binary disorder, studied in the present work. In Sec. III, the physics of the Mott-insulator (MI) phases is explained and their phase-boundaries are calculated by employing perturbation theory with respect to the hopping amplitude. Section IV deals with exact numerical calculations of the many-particle ground states for small lattices. In Sec. V, we consider a one-dimensional system in the limit of strong interaction, which is exactly solvable through the Bose-Fermi mapping. A summary of the work is given in Sec. VI.

## II. HAMILTONIAN

We consider a system of ultracold interacting bosons in a  $d$ -dimensional hypercubic lattice described by the Bose-Hubbard Hamiltonian

$$\hat{H} = -J \sum_{\langle i,j \rangle} \hat{a}_i^\dagger \hat{a}_j + \frac{U}{2} \sum_i \hat{a}_i^\dagger \hat{a}_i^\dagger \hat{a}_i \hat{a}_i + \sum_i (\epsilon_i - \mu) \hat{a}_i^\dagger \hat{a}_i, \quad (1)$$

where  $J$  is the tunneling matrix element for the nearest lattice sites,  $U$  is the on-site atom-atom interaction energy, and  $\mu$  is the chemical potential. Throughout the paper, we will be dealing with repulsive interaction, i.e.,  $U > 0$ . We assume periodic boundary conditions. The annihilation and creation operators,  $\hat{a}_i$  and  $\hat{a}_i^\dagger$ , obey the bosonic commutation relations.

The disorder described by the random terms  $\epsilon_i$  is assumed to be created by the presence of impurity atoms located at fixed random positions (quenched disorder). This type of disorder is diagonal in the sense that it does not lead to any contributions to the hopping term. If it has a “fermionic” character, i.e., if there is at most one impurity at each lattice site, the probability distribution of on-site energies  $\epsilon_i$  is given by

$$p(\epsilon) = p_0\delta(\epsilon) + (1-p_0)\delta(\epsilon-U'), \quad p_0 = (L-L')/L, \quad (2)$$

with  $0 \leq p_0 \leq 1$ , where  $U'$  is the boson-impurity interaction energy.  $L$  is the number of lattice sites and  $L'$  is the number of impurities.  $p_0 = 1$  or  $U' = 0$  corresponds to the pure case. The binary disorder distribution (2) implies that the system under consideration remains invariant under the transformation  $p_0 \rightarrow 1 - p_0$ ,  $U' \rightarrow -U'$ . This can be easily seen if we subtract  $U'/2$  from the on-site energies  $\epsilon_i$ , i.e., if we make the replacement  $\epsilon \rightarrow \epsilon + U'/2$  on the r.h.s. of Eq. (2). Therefore, it is enough to consider the case  $U' \geq 0$ .

### III. STRONG-COUPLING EXPANSION

It is known that the Bose-Hubbard model with continuous disorder distribution possesses a rich phenomenology of phases resulting in a nontrivial phase diagram [21]. For the present case of binary disorder, we determine the zero temperature phase diagram next. The physics of the MI phases can be understood and their phase boundaries be calculated with a good accuracy by treating the hopping term in the Hamiltonian (1) as a perturbation [22]. This can be done in arbitrary spatial dimensions and, in this section, we will not impose any restrictions with respect to the dimensionality  $d$ . For the binary disorder distribution (2) it is convenient to consider the entire lattice as consisting of two disconnected sublattices  $\mathcal{L}_0$  and  $\mathcal{L}_1$ . The sublattice  $\mathcal{L}_1$  consists of the  $L'$  potential wells which are shifted by  $\epsilon_i = U'$  with respect to the wells of the other sublattice  $\mathcal{L}_0$ . In what follows, it is assumed that  $0 < p_0 < 1$ . One may then define the local chemical potentials of the sublattices  $\mathcal{L}_0$  and  $\mathcal{L}_1$  as  $\mu$  and  $\mu - U'$ , respectively. The special case of a pure lattice can be retrieved in the limit  $U' \rightarrow 0$ .

In the limit of vanishing hopping ( $J = 0$ ), the states of the system are characterized by the occupation numbers of each lattice site. In the ground state corresponding to the MI, we have  $n_0$  bosons at each site of the sublattice  $\mathcal{L}_0$ , and  $n_1$  bosons at each site of the sublattice  $\mathcal{L}_1$ , where  $n_0$  and  $n_1$  are the smallest non-negative integers larger than or equal to  $\mu/U$  and  $(\mu - U')/U$ , respectively. In general,  $n_1 \leq n_0$  and the total number of bosons  $N$  is given by  $N = n_0(L - L') + n_1L'$ . We are interested in the thermodynamic limit  $N \rightarrow \infty$ ,  $L \rightarrow \infty$ ,  $L' \rightarrow \infty$ , where  $N/L$  as well as  $p_0$  remain finite. The particle and hole excitations in the limit of infinite lattices are localized within the Lifshitz rare regions [25] which consist of infinitely large connected regions of either sublattice  $\mathcal{L}_0$  or  $\mathcal{L}_1$  depending on the disorder parameter  $U'$  and the chemical potential  $\mu$ . This allows us to work out the boundaries of the MI regions by generalizing the method of strong-coupling expansion developed in Ref. [26]. Due to the infinite extent

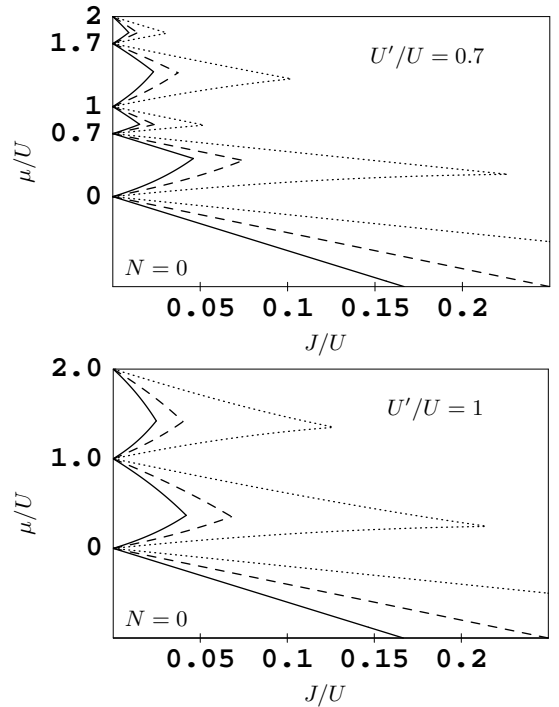


FIG. 1: The boundaries of the MI phases obtained by the strong-coupling expansion in  $d = 1$  (dotted), 2 (dashed), 3 (solid) for  $U'/U = 0.7$  (top) and for  $U'/U = 1$  (bottom).

of the Lifshitz rare regions, the boundaries of the MI regions should not depend on  $p_0$ . This dependence appears as a finite size effect which we do not consider in this section.

The region  $\mu < -2dJ$  corresponds to a vanishing particle number  $n_0 = n_1 = 0$ . The intervals  $n_0 - 1 < \mu/U < n_0$ ,  $n_0 = 1, \dots, [U'/U]$ , with  $[\dots]$  denoting the integer part, correspond to the MI with  $n_1 = 0$ . The lowest-energy particle-hole excitations are created by transferring one atom among the lattice sites of the sublattice  $\mathcal{L}_0$ . The energy gap for the creation of this excitation equals  $U$  at  $J = 0$ . The MI phases are enclosed in the interval  $\mu_h(n_0) < \mu < \mu_p(n_0)$ , where

$$\begin{aligned} \mu_p(n) &= Un - 2dJ(n+1) \\ &+ \frac{J^2}{U}n [d(5n+4) - 4d^2(n+1)] \\ &+ \frac{J^3}{U^2}n(n+1) [-8d^3(2n+1) + d^2(25n+14) \\ &\quad - 4d(2n+1)] + O(J^4), \\ \mu_h(n) &= U(n-1) + 2dJn \\ &- \frac{J^2}{U}(n+1) [d(5n+1) - 4d^2n] \\ &+ \frac{J^3}{U^2}n(n+1) [8d^3(2n+1) - d^2(25n+11) \\ &\quad + 4d(2n+1)] + O(J^4), \end{aligned} \quad (3)$$

are the boundaries of the MI phase in the pure case [26].

The next intervals  $n_0 - 1 < \mu/U < n_0$ , where  $n_0 = [U'/U] + 1, \dots$ , are split into two subintervals. In the lower

subinterval  $n_0 - 1 < \mu/U < n_0 - 1 + \{U'/U\}$ , where  $\{\dots\}$  denotes the fractional part,  $n_1 = n_0 - [U'/U] - 1$ . The lowest-energy particle-hole excitation of this state can be created by transferring one atom from the sublattice  $\mathcal{L}_0$  to the sublattice  $\mathcal{L}_1$ . As a result of this transfer, the energy of the initial state is increased by  $U \{U'/U\}$ . Perturbative calculations in the thermodynamic limit show that it is located in the interval  $\mu_h(n_0) < \mu < U' + \mu_p(n_1)$  of the phase diagram (Fig. 1).

In the upper subinterval  $n_0 - 1 + \{U'/U\} < \mu/U < n_0$ ,  $n_1 = n_0 - [U'/U]$ . The lowest-energy particle-hole excitation of this state can be created by transferring one atom from the sublattice  $\mathcal{L}_1$  to the sublattice  $\mathcal{L}_0$ . As a result of this transfer, the energy of the initial state is increased by  $U - U \{U'/U\}$ . According to the perturbation theory, it is located in the interval  $U' + \mu_h(n_1) < \mu < \mu_p(n_0)$ , where  $\mu_h(n)$  and  $\mu_p(n)$  are given by Eq. (3).

The two subintervals exist only if  $\{U'/U\}$  does not vanish, otherwise the lower subinterval disappears. The upper one then becomes extended from  $\mu = (n_0 - 1)U$  to  $\mu = n_0 U$ . In this case, it is energetically more favorable to create the particle-hole excitations by transferring one atom among the lattice sites of the sublattice  $\mathcal{L}_0$  and the MI phase is enclosed within the interval  $\mu_h(n_0) < \mu < \mu_p(n_0)$ .

MI phases with equal occupation numbers  $n_0 = n_1 = n$  exist only for  $0 \leq U'/U < 1$ , i.e.,  $[U'/U] = 0$  and  $\{U'/U\} = U'/U$ . They are located within the intervals  $n_0 - 1 + U'/U < \mu/U < n_0$ .

The MI regions for  $U'/U = 0.7$  and for  $U'/U = 1$  are shown in Fig. 1. In the case  $U'/U = 0.7$ , we have only split MI regions with  $n_0 = 1, 2, \dots$ , where the lower and upper parts correspond to  $n_1 = n_0 - 1$  and  $n_1 = n_0$ , respectively. In the case  $U'/U = 1$ , there are only nonsplit MI regions with  $n_1 = n_0 - 1$ . With the increase of the dimensionality  $d$ , the MI regions become smaller.

Since we are dealing with a disordered system, one can expect the existence of the Bose-glass (BG) phase [21]. However, the method of strong-coupling expansion in its present form does not allow us to detect the corresponding regions on the phase diagram. It does not give the opportunity to investigate the temperature-dependent effects either. Therefore, other methods are needed in order to study the complete phase diagram of the system. They are employed in the next sections, where we consider only one-dimensional lattices.

#### IV. EXACT DIAGONALIZATION

In this section we study zero-temperature properties of the system by means of exact numerical diagonalization of the Bose-Hubbard Hamiltonian along the lines of Ref. [27]. For this we determine first the boundaries of the regions in the  $(\mu, J)$  plane corresponding to different total particle numbers  $N$ . This requires calculations of the ground-state energies  $E_N$  of the Hamiltonian (1) for different  $N$  and can be done exactly with the aid of iterative numerical solvers for sparse matrices of large dimensions.

The results of these calculations for a small one-dimensional lattice are presented in Fig. 2. The solid lines

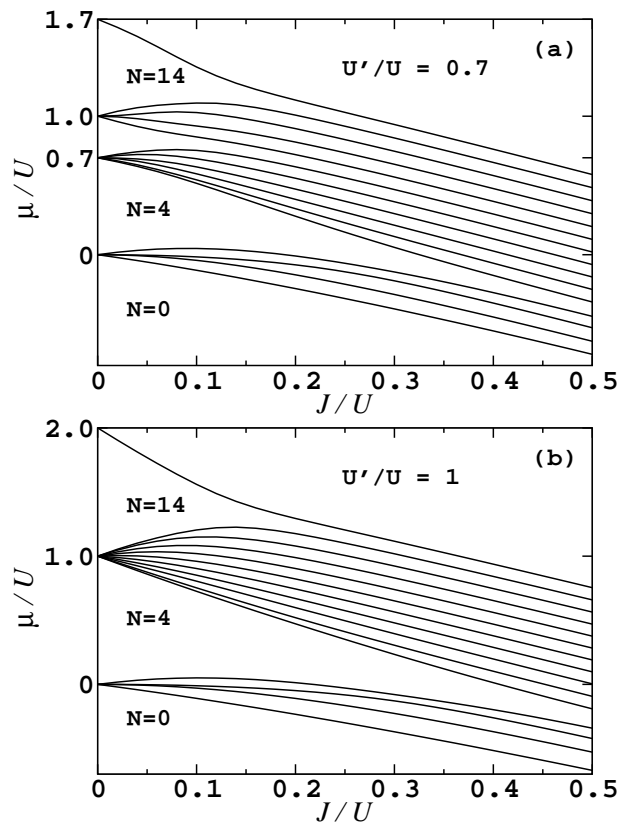


FIG. 2: The regions with occupation numbers  $N = 0, \dots, 14$  obtained by the exact diagonalization of the Hamiltonian (1) for  $L = 10$ ,  $L' = 6$  for one disorder realization characterized by the Fock state  $|0011101011\rangle$  for  $U'/U = 0.7$  (a) and for  $U'/U = 1$  (b).

indicate the boundaries  $\mu_N = E_N - E_{N-1}$  of the regions with different occupation numbers  $N$  of the lattice. These calculations are performed for  $L = 10$  and  $L' = 6$  and for one disorder realization, where the spatial distribution of impurities is described by the Fock state  $|0011101011\rangle$ . The maximal number of bosons is 15. The lowest line is the boundary between  $N = 0$  and  $N = 1$ , the next one is the boundary between  $N = 1$  and  $N = 2$  and so on.

In the case  $U'/U = 0.7$  (Fig. 2a), the regions with the occupation numbers  $N = L - L' = 4$ ,  $N = L = 10$ ,  $N = 2L - L' = 14$  appear to be larger than the others indicating that there are MI phases for these occupations. In spite of the large contribution of the finite-size effects, the shape of these regions is in good agreement with the results of the strong-coupling expansion, see Fig. 1.

As it was discussed in the previous section, the MI phases with integer filling factors disappear if  $U' \geq U$  and only the MI phases with incommensurate fillings remain. This behavior can be also seen in Fig. 2b.

With the increase of the number of lattice sites  $L$ , the boundaries of the regions with different occupation number are closer to each other and in the thermodynamic limit they should densely cover the whole  $(\mu, J)$  plane except the MI regions. In order to really see this transition to the thermody-

dynamic limit as well as to determine the boundaries of the MI regions, one has to vary the number  $L$  of lattice sites and the number  $N$  of bosons in a wide range which is difficult here because the dimension of the bosonic Hilbert space grows exponentially with  $N$  and  $L$ .

The fraction  $f_s^N$  of the total atom number  $N$  which are in the superfluid phase (superfluid fraction) can be calculated with the aid of Peierls phase factors. They have to be introduced in the Hamiltonian (1) by means of the replacement  $\hat{a}_i^\dagger \hat{a}_{i+1} \rightarrow \hat{a}_i^\dagger \hat{a}_{i+1} e^{i\phi}$ . By calculating the free energy  $F_N(\phi)$  for some small value of  $\phi$ , the superfluid fraction is determined as [27, 28]

$$f_s^N = \lim_{\phi \rightarrow 0} \frac{F_N(\phi) - F_N(0)}{J\phi^2 N}. \quad (4)$$

The limit  $\phi \rightarrow 0$  can be calculated exactly if the complete solution of the eigenvalue problem is known (see Ref. [27] and the discussion in Sec. V A). However, all the numerical solvers for large sparse matrices allow efficient calculations only of a small number of the eigenstates. This is the reason why the superfluid fraction defined by Eq. (4) is usually worked out for some small but nonvanishing value of  $\phi$ .

The behavior of  $f_s^N$  for different  $N$  is shown in Fig. 3 for the same fixed disorder realization as above. In these calculations,  $\phi = 0.01$ . In the case  $U'/U = 0.7$ , the superfluid fraction vanishes not only for fillings which allow the existence of the MI phases ( $N = 4, 10, 14$ ) but also for all the others if the hopping parameter  $J$  is small enough. This suggests a phase transition from the superfluid into the BG phase. The case  $U'/U = 1$  looks different. The superfluid fraction vanishes only for  $N = 1, 2, 3, 4, 14$  and remains finite for all the others, even for small values of  $J/U$ . This suggests that the BG phase exists in the extended regions of the  $(\mu, J)$  plane corresponding to low fillings but is strongly suppressed for higher fillings.

Since exact diagonalization can be performed only for very small lattices, it is difficult to provide a satisfactory description of the phase diagram of the system. Finite-size effects can be much better controlled in the case of hard-core bosons, which is treated in the next section.

## V. BOSE-FERMI MAPPING

We consider the hard-core limit of infinitely strong repulsion  $U \rightarrow \infty$  in a one-dimensional lattice, which is exactly solvable via the Jordan-Wigner transformation [29, 30]

$$\hat{a}_l = \exp\left(i\pi \sum_{j<l} \hat{c}_j^\dagger \hat{c}_j\right) \hat{c}_l \quad (5)$$

where  $\hat{c}_l$  and  $\hat{c}_l^\dagger$  are the fermionic annihilation and creation operators. Under this transformation the Hamiltonian (1) takes the form

$$\hat{H} = -J \sum_{i=1}^L \left( \hat{c}_i^\dagger \hat{c}_{i+1} + \hat{c}_{i+1}^\dagger \hat{c}_i \right) + \sum_{i=1}^L (\epsilon_i - \mu) \hat{c}_i^\dagger \hat{c}_i. \quad (6)$$

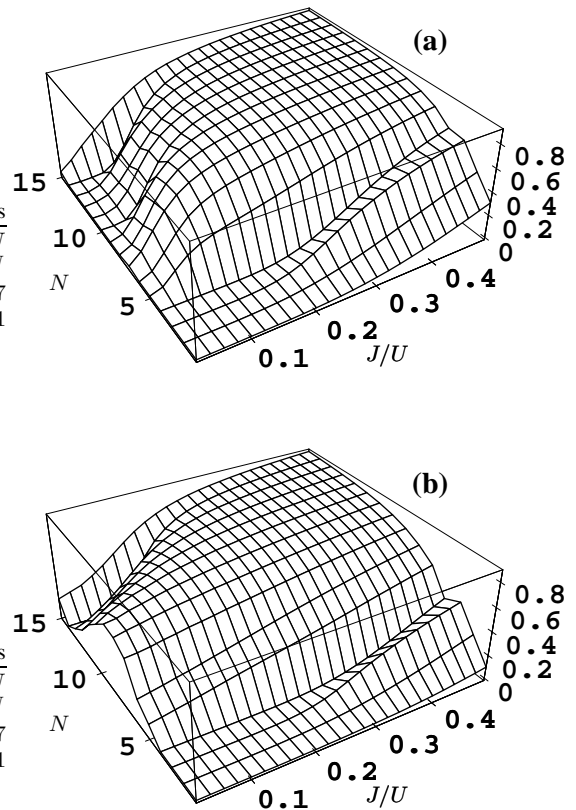


FIG. 3: Superfluid fraction  $f_s^N$  vs  $N$  and  $J$  obtained by exact diagonalization for  $L = 10$ ,  $L' = 6$  for  $U'/U = 0.7$  (a) and for  $U'/U = 1$  (b). The points for different values of  $N$  are connected in order to guide eyes.

Periodic boundary conditions for bosons are equivalent to the requirement

$$\hat{c}_{L+1} = \exp\left(-i\pi \sum_{j=1}^L \hat{c}_j^\dagger \hat{c}_j\right) \hat{c}_1, \quad (7)$$

which implies periodic boundary conditions for fermions if the number of particles  $N$  is odd, otherwise one should use the corresponding antiperiodic boundary conditions in the Hamiltonian (6).

The  $N$ -particle eigenstates of the Hamiltonian (6) can be constructed from the  $L$  single-particle eigenstates as

$$|\alpha\rangle = \sum_{i=1}^L \varphi_\alpha(i) \mathcal{T}^{i-1} |\underbrace{10\dots 0}_L\rangle \quad (8)$$

with the eigenenergies  $\epsilon_\alpha$ ,  $\alpha = 1, \dots, L$ . Here,  $\mathcal{T}$  is the translation operator. Its action  $\mathcal{T}^i$  on the one-particle Fock state  $|10\dots 0\rangle$  results in the shift of the particle's position by  $i$  lattice sites. This allows to treat much larger lattices compared to the case of soft-core bosons considered in Sec. IV. However,

one still cannot avoid numerics because the analytical solution of the single-particle eigenvalue problem in the presence of disorder is not known.

In the infinite- $U$  limit, the occupation numbers of the individual lattice sites can be 0 or 1 implying that the maximal number of atoms  $N$  cannot be larger than  $L$ . The state with  $N = L$  is always a MI as no hopping can take place any more and a non-trivial treatment of the MI phase in the hard-core limit is possible only for  $N < L$ .

### A. Bose-Einstein condensation and superfluidity

Before starting the discussion of the remaining part of the phase diagram, some remarks on the Bose-Einstein condensation (BEC) and superfluidity of hard-core bosons in 1D are in order. In the absence of disorder, the spatial correlation function  $\langle \hat{a}_i^\dagger \hat{a}_j \rangle$  in the limit  $|i - j| \rightarrow \infty$  decays as  $|i - j|^{-1/2}$ . The presence of disorder makes this decay faster, i.e., there is no off-diagonal long-range order and BEC [31].

The absence of BEC does not exclude in general the superfluidity. As it was shown in Ref. [32] for the Gaussian disorder, the system of one-dimensional soft-core bosons is in the delocalized (superfluid) state, if the correlation function  $\langle \hat{a}_i^\dagger \hat{a}_j \rangle$  for large distances decays slower than  $|i - j|^{-1/3}$  which leads to the divergence of the localization length. Since the correlation function of hard-core bosons with disorder decays faster than  $|i - j|^{-1/2}$ , the criterion of Ref. [32] excludes the existence of the superfluid phase. The question is whether this remains true for the binary disorder.

The superfluid fraction is defined by Eq. (4). The limit  $\phi \rightarrow 0$  can be calculated making use of the perturbative approach of Ref. [27]. For hard-core bosons in 1D, this leads to the following general expression at  $T = 0$ :

$$f_s^N = \frac{1}{2N} \sum_{i=1}^L \sum_{\alpha=1}^N [\varphi_\alpha^*(i) \varphi_\alpha(i+1) + c.c.] \quad (9)$$

$$- \frac{J}{N} \sum_{\alpha=N+1}^L \sum_{\beta=1}^N \frac{1}{\varepsilon_\alpha - \varepsilon_\beta}$$

$$\times \left| \sum_{i=1}^L [\varphi_\alpha^*(i) \varphi_\beta(i+1) - \varphi_\alpha^*(i+1) \varphi_\beta(i)] \right|^2,$$

where  $\varphi_\alpha(L+1) = (-1)^{N+1} \varphi_\alpha(1)$ . In the clean case, the second term in Eq. (9) vanishes and in the thermodynamic limit we get  $f_s = \frac{\sin \pi n}{\pi n}$ , where  $n = N/L$  [33]. This result does not depend on  $J$ .

The results of numerical calculations for the binary disorder are shown in Fig. 4 for  $J/U' = 1$  for two different lattice sizes. Here and later on the overline indicates the disorder-averaged quantity. For a small lattice size  $L = 100$ ,  $f_s$  appears to be finite. However, when increasing  $L$  to  $L = 200$ ,  $f_s$  approaches zero. For smaller values of  $J/U'$ , smaller lattice sizes  $L$  are sufficient in order to see that  $f_s$  indeed vanishes in the thermodynamic limit, i.e., we expect only insulating phases in our system. For comparison, the corresponding result for the clean case is also shown in Fig. 4, see dashed line.

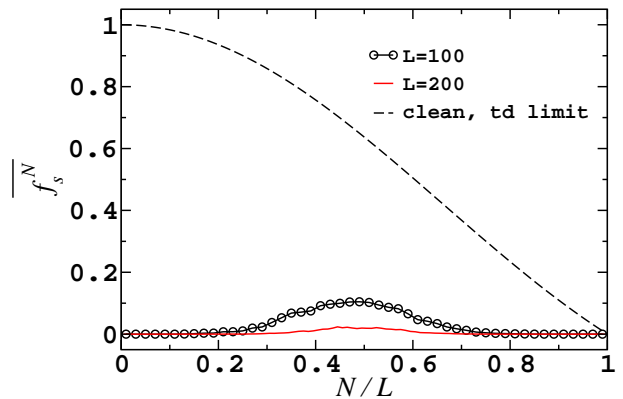


FIG. 4: Superfluid fraction for  $J/U' = 1$ ,  $L' = L/2$ ,  $L = 100$  (circles), 200 (solid line) averaged over 400 disorder realizations. The dashed line shows the superfluid fraction in the thermodynamic limit without disorder, i.e.,  $f_s = \frac{\sin(\pi N/L)}{\pi N/L}$ , see text.

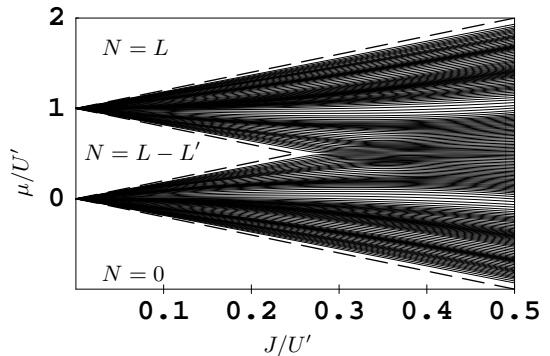


FIG. 5: The regions with occupation numbers  $N = 0, \dots, L$  obtained by the exact diagonalization of the Hamiltonian (6) for  $L = 200$ ,  $L' = 100$ . The results are averaged over 400 disorder realizations. Dashed lines are analytical results for the boundaries of the MI regions in the thermodynamic limit.

Since the hard-core limit works for  $U'/U < 1$  and  $J/U \ll 1$ , this qualitatively agrees with the behavior of  $f_s^N$  for  $N \leq L = 10$  and relatively small  $J/U$  calculated by means of exact diagonalization in the case of soft-core bosons (Fig. 3a).

### B. Quantum phases

The boundaries of the MI-regions at zero temperature can be easily calculated analytically in the thermodynamic limit following the general treatment of Sec. III for  $d = 1$ ,  $U' < U$ . The region  $\mu < -2J$  contains no atoms. The MI phases with non-integer filling factors are located in the interval  $\mu_h(n_0) < \mu < U' + \mu_p(n_1)$ , where  $n_0 = 1$ ,  $n_1 = 0$ . In the limit  $U \rightarrow \infty$ , all the terms in Eq. (3) proportional to  $J^p$  with  $p > 1$  vanish and we get explicitly  $2J < \mu < U' - 2J$ , where  $J < U'/4$ .  $U' + \mu_h(n_1) < \mu < \mu_p(n_0)$  with  $n_0 = n_1 = 1$ , i.e.,  $U' + 2J < \mu < \infty$  corresponds to the MI with  $N = L$ . These results are shown in Fig. 5 by dashed lines.

The same boundaries as well as the boundaries of the re-

gions with different occupation numbers  $\mu_N$  can be calculated numerically by means of exact diagonalization.  $\mu_N$  are equal to the single-particle eigenenergies  $\varepsilon_N$  because the ground-state energy of  $N$  non-interacting fermions is the sum of  $N$  lowest single-particle eigenenergies. The region  $\mu < \varepsilon_1$  contains no atoms. The MI phase with  $L - L'$  atoms is located in the interval  $\varepsilon_{L-L'} < \mu < \varepsilon_{L-L'+1}$ . If  $\mu > \varepsilon_L$ , we have the MI with  $N = L$ . The boundaries  $\varepsilon_1, \dots, \varepsilon_L$  are shown by solid lines in Fig. 5 for  $L = 200$ . The lines  $\varepsilon_1, \varepsilon_{L-L'}, \varepsilon_{L-L'+1}, \varepsilon_L$  are outside of the corresponding regions determined in the thermodynamic limit, similar to what is seen in Fig. 2. They come closer to the results obtained in the limit  $L \rightarrow \infty$  if the lattice size  $L$  is increased.

The distribution of lines  $\mu_N = \varepsilon_N(J)$ ,  $N = 1, \dots, L$ , in Fig. 5 is very inhomogeneous which leads to the fact that the compressibility of the system varies in a rather wide range. This characteristic feature remains preserved for larger lattices as well and it is easier to see it in the behavior of  $N(\mu)$  which is given by

$$N(\mu) = \sum_{\alpha=1}^L f(\varepsilon_\alpha), \quad f(\varepsilon) = \frac{1}{\exp[(\varepsilon - \mu)/k_B T] + 1}. \quad (10)$$

The plots  $N(\mu)$  at  $T = 0$  are shown in Fig. 6a. The central plateaus ( $N = L - L'$ ) around  $\mu/U' = 0.5$  which exist for  $J/U' < 0.25$  correspond to the MI phase. Quasi-plateaus of  $N(\mu)$  which exist at any values of  $J/U'$  correspond to the regions on the  $(J, \mu)$ -diagram with low density of lines  $\mu_N(J)$ .

In order to clarify the physical interpretation of different parts of the phase diagram, we have calculated the time-dependent Green's function  $G(\tau) = \langle \hat{a}_i(\tau) \hat{a}_i^\dagger(0) \rangle$  defined for  $\tau > 0$  which determines the density of states of the single-particle excitations as well as the superfluid susceptibility [21]. The plots of  $G(\tau)$  as a function of the imaginary time  $\tau$  are shown in Fig. 7. In the MI phase,  $G(\tau)$  at large  $\tau$  is an exponential function of  $\tau$ . This also holds for  $N = L - L'$ ,  $J/U' < 0.25$ . If the number of particles remains the same but  $J/U'$  is increased, the exponential decay of  $G(\tau)$  is replaced by the  $1/\tau$ -law indicating that now we are in the BG phase (Fig. 7 main) according to Ref. [21].  $1/\tau$ -law is also observed for other particle numbers corresponding to the quasi-plateaus of  $N(\mu)$  (inset of Fig. 7) which allows to interpret them as belonging to the BG phase, in spite of the fact that the compressibility is extremely small.

The density of states for the single-particle excitations can be determined in terms of the Fourier transformed single-particle Green's function  $\tilde{G}(E)$  as  $\rho(E) = -\frac{1}{\pi} \text{Im} \tilde{G}(E)$  [23]. For hard-core bosons, it takes the form

$$\rho(E) = \sum_{\alpha, \beta} f(\varepsilon_\alpha) [1 - f(\varepsilon_\beta)] \delta(E - \varepsilon_\beta + \varepsilon_\alpha), \quad (11)$$

where  $\varepsilon_\beta - \varepsilon_\alpha$  are the energies of single-particle excitations caused by the transfer of one particle from the energy level  $\varepsilon_\alpha$  to the energy level  $\varepsilon_\beta$ .

Numerical calculations were performed assuming that the energy levels have a finite lifetime. The  $\delta$ -function is approximated by a Gaussian with the standard deviation  $0.01U'$ . The

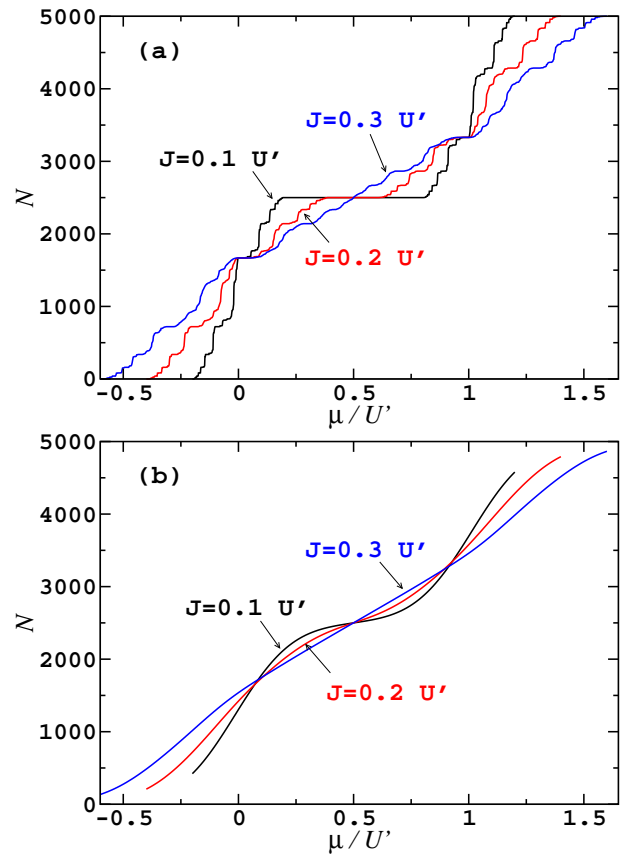


FIG. 6: (Color online)  $N(\mu)$  in the hard-core limit for  $k_B T/U' = 0$  (a), 0.1 (b) and for one disorder realization which is the same in (a) and (b).  $L = 5000$ ,  $L' = 2500$ ,  $J/U' = 0.1$  (black), 0.2 (red), 0.3 (blue).

disorder-averaged energy dependences at  $T = 0$  are shown in Fig. 8 for different values of  $J$ .  $\bar{\rho}(E)$  has always a multi-maxima structure which stems from the inhomogeneous distribution of the single-particle eigenenergies (see Figs. 5, 6a).

The density of excited states at  $E = 0$  as a function of  $J$  is shown in Fig. 9 for  $N = L - L'$ .  $\rho(0)$  vanishes for  $J/U' \lesssim 0.25$ , and is different from zero otherwise. For other particle numbers,  $\rho(0)$  does not vanish for any  $J$ . This is directly related to the asymptotic properties of the time-dependent Green's function  $G(\tau)$  discussed above.  $\rho(0) > 0$  is a clear-cut signature of the BG [21, 24].

At finite temperature,  $N(\mu)$  defined in Eq. (10) becomes a smooth function (Fig. 6b). The MI plateaus which are clearly seen for  $J/U' = 0.1, 0.2$  at  $T = 0$  (Fig. 6a) are smeared out and the quasi-plateaus disappear even at rather small  $T$  indicating that the compressibility never vanishes. Nevertheless, one can say that the MI still exists as long as the gap for the creation of particle-hole excitations, which is  $U' - 4J$  in the case of hard-core bosons in 1D, is larger than the thermal energy  $k_B T$ . This suggests that the upper and lower boundaries of the MI-region are given by  $U' - 2J - k_B T/2$  and  $2J + k_B T/2$ , respectively, and the crossover line for the MI on the  $(J, T)$ -diagram is given by  $k_B T_c^{MI} = U' - 4J$ .

If temperature is increased, quantum statistics will become

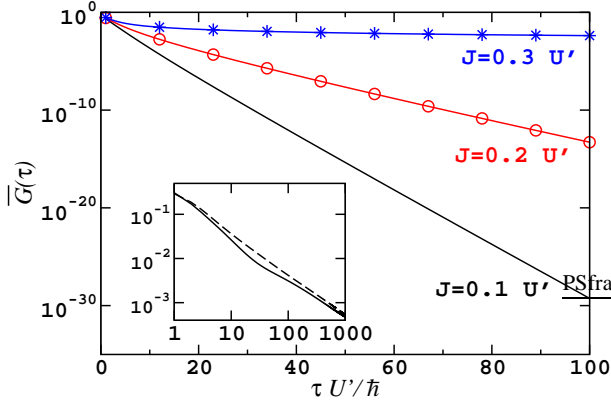


FIG. 7: (Color online) Linear-log plot of  $\bar{G}(\tau)$  for  $L = 400$  averaged over 5000 disorder realizations for  $N = 200$  and  $J/U' = 0.1$  (black solid),  $J/U' = 0.2$  (red circles) and  $J/U' = 0.3$  (blue stars). Inset: same in a log-log plot for  $J/U' = 0.3$  for  $N = 132$  (solid) and  $N = 200$  (dashed) which corresponds to  $\mu/U' \approx 0$  and  $0.5$ , respectively.

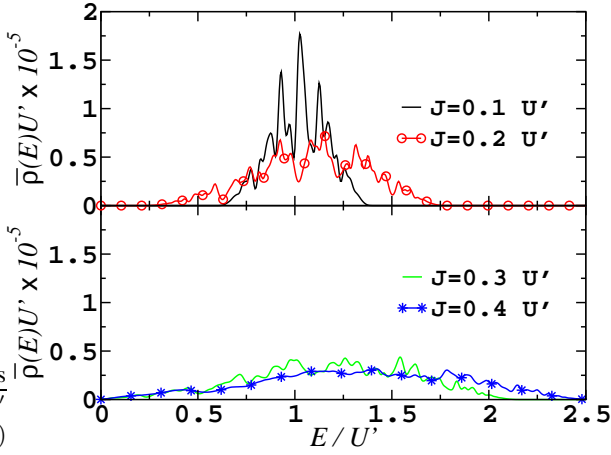


FIG. 8: (Color online) Density of excited states at  $T = 0$  averaged over 200 disorder realizations.  $L = 400$ ,  $L' = 200$ ,  $N = 200$ ,  $J/U' = 0.1$  (black),  $0.2$  (red),  $0.3$  (green),  $0.4$  (blue).

less important and one can expect that the MI phase as well as the BG phase is destroyed. Then, a crossover into the normal-gas state is expected. Since the thermodynamic properties of hard-core bosons are equivalent to those of the ideal Fermi gas, the crossover temperature coincides with the Fermi temperature modified by the disorder.

### C. Experimentally measurable quantities

The Bose-Fermi mapping allows very detailed investigations of different physical properties of the system which can be directly measured in experiments. We consider first the momentum distribution [34]

$$\langle \tilde{\psi}^\dagger(k) \tilde{\psi}(k) \rangle = \left| \tilde{W}(k) \right|^2 \frac{1}{N} \sum_{l,l'} \exp[ika(l-l')] \langle \hat{a}_l^\dagger \hat{a}_{l'} \rangle,$$

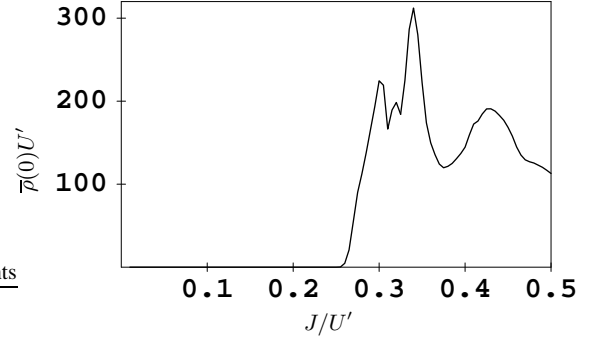


FIG. 9: Density of excited states at  $T = 0$  and  $E = 0$  averaged over 200 disorder realizations.  $L = 400$ ,  $L' = 200$ ,  $N = 200$ .

where  $k$  is the wavenumber,  $a$  is the lattice constant, and  $\tilde{W}(k)$  is the Fourier transform of the Wannier function  $W(x)$  for the lowest Bloch band of the lattice potential. The matrix elements  $\langle \hat{a}_l^\dagger \hat{a}_{l'} \rangle$  of the  $L \times L$  one-particle density matrix can be worked out for  $l > l'$  as a determinant of the  $(l-l') \times (l-l')$  Toeplitz matrix  $G^{(l,l')}$  [30, 31] as

$$\langle \hat{a}_l^\dagger \hat{a}_{l'} \rangle = 2^{l-l'-1} \det G^{(l,l')}. \quad (12)$$

The matrix elements of  $G^{(l,l')}$  are given by

$$G_{i,j}^{(l,l')} = \langle c_{l-j+1}^\dagger c_{l-i} \rangle - \frac{1}{2} \delta_{j,i+1}. \quad (13)$$

The expectation values  $\langle c_i^\dagger c_j \rangle$  can be calculated using the solution of the single-particle eigenvalue problem as

$$\langle c_i^\dagger c_j \rangle = \sum_{\alpha=1}^L \varphi_\alpha^*(i) \varphi_\alpha(j) f(\varepsilon_\alpha). \quad (14)$$

The momentum distributions obtained by numerical calculations for  $N = L - L'$  are shown in Fig. 10. In general,  $P(k) = \langle \tilde{\psi}^\dagger(k) \tilde{\psi}(k) \rangle / |\tilde{W}(k)|^2$  is an even and periodic function of  $ka$  with the period  $2\pi$ . It takes maximal (minimal) values at  $ka = \pi m$ ,  $m = 0, \pm 2, \pm 4, \dots$  ( $m = \pm 1, \pm 3, \dots$ ). With the decrease of the hopping parameter  $J$  the spatial correlations of bosons become weaker which leads to the broadening of the momentum distribution. As discussed above, for  $N = L - L'$  the system undergoes a phase transition from the BG to MI, where the spatial correlation functions obey power and exponential laws, respectively. Therefore, the dependence of the momentum distribution on  $J$  is expected to be weaker in the MI than in the BG, which is demonstrated in Fig. 10. The transition point is seen as a kink in the  $J$ -dependence of the momentum distribution function at  $k = 0$  (inset of Fig. 10). For  $N = (L - L')/2$ , which always corresponds to the BG phase, the dependence is almost linear without any kink.

At finite temperature, the qualitative form of the momentum distribution remains unchanged. As shown in Fig. 11,  $\bar{P}(0)$  is a decreasing function of  $T$  for large enough  $J/U'$  corresponding to the BG region in the phase diagram at  $T = 0$ . The largest choice  $J = 0.4U'$  is in the BG-region rather far from

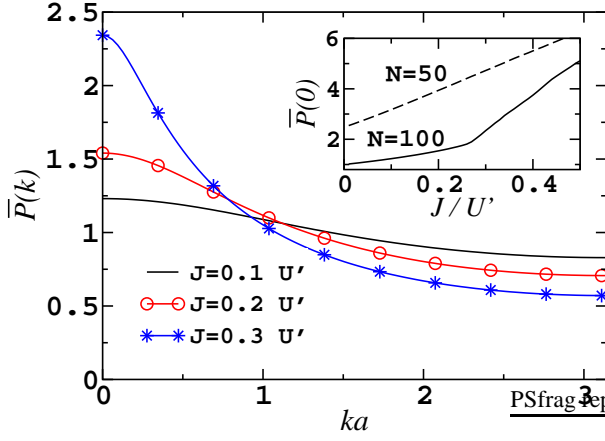


FIG. 10: (Color online) Momentum distribution in the hard-core limit at  $T = 0$  averaged over 200 disorder realizations for  $L = 200$ ,  $L' = 100$ ,  $N = 100$ . Inset: Maximum of the momentum distribution.

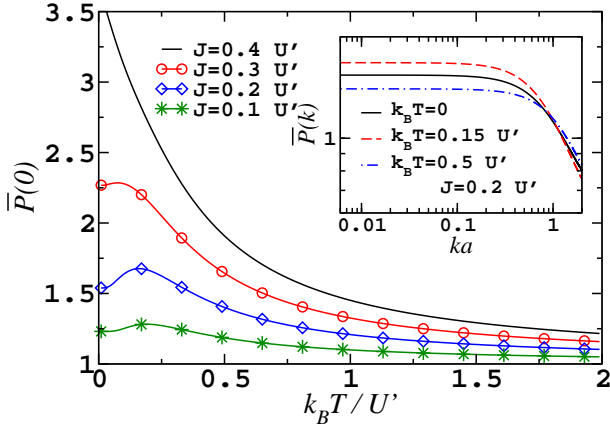


FIG. 11: (Color online) Temperature dependence of  $\bar{P}(0)$  for  $L = 200$ ,  $L' = 100$ ,  $N = 100$  averaged over 250 disorder realizations. Inset: Log-log plot of  $\bar{P}(k)$  for the same parameters.

the BG-MI transition point implying that the averaged momentum distribution has a tendency to become broader due to the influence of the thermal fluctuations. For smaller values of  $J/U'$ , i.e., closer to the BG-MI transition,  $\bar{P}(0)$  first increases for small  $T$  and then decreases further. For the smallest value  $J = 0.1U'$ , the system is deep in the MI phase at  $T = 0$ , and the intermediate maximum in  $\bar{P}(0)$  as a function of  $T$  vanishes again.

Useful information about the state of the many-body system can be obtained with the aid of Bragg spectroscopy [35, 36]. The response of the system to this kind of measurement is described by the dynamical structure factor, which is defined as

$$S(k, \omega) = \int_{-\infty}^{\infty} dt \langle \Delta\tilde{\rho}(k, 0) \Delta\tilde{\rho}(-k, t) \rangle \exp(-i\omega t), \quad (15)$$

where  $\Delta\tilde{\rho}(k)$  is the spatial Fourier transform of the density-fluctuation operator. In the case of deep lattices it takes the

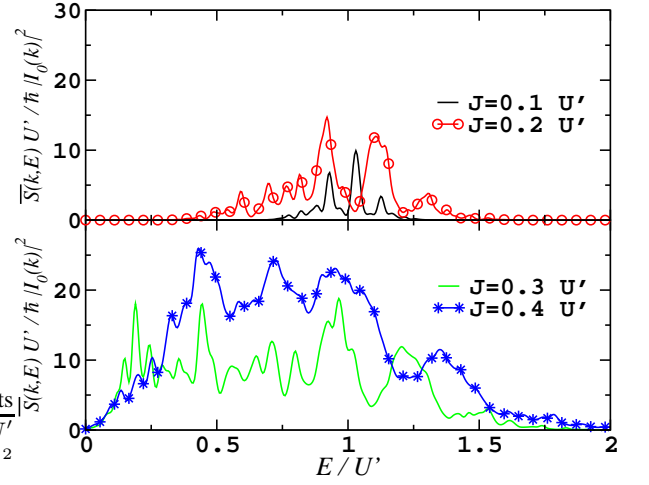


FIG. 12: (Color online) Dynamical structure factor in the hard-core limit at  $T = 0$  averaged over 600 disorder realizations. Parameters are  $L = 200$ ,  $L' = 100$ ,  $N = 100$ ,  $ka = \pi/3$ . Moreover,  $J/U' = 0.1$  (black),  $0.2$  (red),  $0.3$  (green),  $0.4$  (blue).

form

$$\Delta\tilde{\rho}(k) = I_0(k) \sum_l \left( a_l^\dagger a_l - \langle a_l^\dagger a_l \rangle \right) \exp(ikal), \quad (16)$$

where

$$I_0(k) = \int_{-\infty}^{\infty} dx \exp(ikx) |W(x)|^2 \quad (17)$$

with  $W(x)$  being the Wannier function for the lowest Bloch band. The dynamical structure factor for hard-core bosons can be expressed in terms of the single-particle eigenmodes as [37]

$$S(k, E) = \hbar |I_0(k)|^2 \sum_{\alpha, \beta} \left| \sum_l \varphi_\alpha^*(l) \varphi_\beta(l) e^{ikal} \right|^2 \times f(\varepsilon_\alpha) [1 - f(\varepsilon_\beta)] \delta(E - \varepsilon_\beta + \varepsilon_\alpha). \quad (18)$$

This formula resembles Eq. (11) for the density of excited states but has a more complicated structure due to the explicit dependence on the mode-functions  $\varphi_\alpha(l)$ .

The resulting dependence of the disorder-averaged dynamical structure factor  $\bar{S}(k, E)$  on energy is shown in Fig. 12 for  $ka = \pi/3$ . The behavior of  $\bar{S}(k, E)$  is completely different compared to the case of homogeneous lattices studied in Ref. [38]. It vanishes in the finite interval of  $E$  near zero, provided that  $J/U' < 0.25$ , due to the energy gap in the excitation spectrum of MI. With the increase of  $J/U'$  the gap decreases. It disappears completely if  $J/U' > 0.25$  due to the transition into the BG phase.  $\bar{S}(k, E)$  is broader in the BG phase ( $J/U' = 0.3, 0.4$ ) than in the MI phase ( $J/U' = 0.1, 0.2$ ). Its multi-peak structure is qualitatively related to the density of excited states, which is shown in Fig. 8. However, the detailed form of the energy dependence of  $S(k, E)$ , which remains preserved for larger lattices as well, is different from

$\rho(E)$  due to the nontrivial contributions of the eigenfunctions  $\varphi_\alpha(i)$  in Eq. (18). The same features are observed for other values of  $ka$ .

Finally, we consider the static structure factor defined as

$$S_0(k) = \int_{-\infty}^{\infty} S(k, E) dE. \quad (19)$$

In the case of hard-core bosons, it is given by Eq. (18), where the  $\delta$ -function is formally replaced by 1. Its  $J$ -dependence is shown in Fig. 13 for  $ka = \pi/3, 2\pi/3$  and  $ka = \pi$ . In general, it grows monotonously with increasing  $J$ . Interestingly enough, we find a kink which corresponds to the MI-BG transition point, similar to the behavior of  $\bar{P}(0)$  in Fig. 10.

## VI. CONCLUSIONS

In the present work, we have studied quantum phase transitions of ultracold bosons with repulsive interaction in a lattice with binary disorder. The system is described by the Bose-Hubbard model with random on-site energies which follow a binary probability distribution. The particular form of disorder is physically realized, e.g., when two species of alkali-metal atoms with different masses are loaded in an optical lattice. The latter is created by counter-propagating laser beams which are strongly detuned from the atomic resonance. If one of the species has a mass, say, 4 times bigger (as it is realized for the combination of  $^{87}\text{Rb}$  and  $^{23}\text{Na}$  atoms), the tunneling of the heavier atoms in a deep enough lattice is suppressed by more than 3 orders of magnitude compared to that of the lighter ones. Thus, they effectively form immobile impurities interacting with the lighter atom species. Larger mass differences, like for the combination of  $^{40}\text{K}$ - $^7\text{Li}$  or  $^{87}\text{Rb}$ - $^7\text{Li}$  and  $^{133}\text{Cs}$ - $^7\text{Li}$ , render the difference in the tunneling rates even more drastic. The impurity atoms then induce an effectively quenched disorder potential for the lighter bosonic atoms. When their number is less than the number of the lattice sites, the probability to find more than one impurity at a lattice site can be extremely low. This is guaranteed by

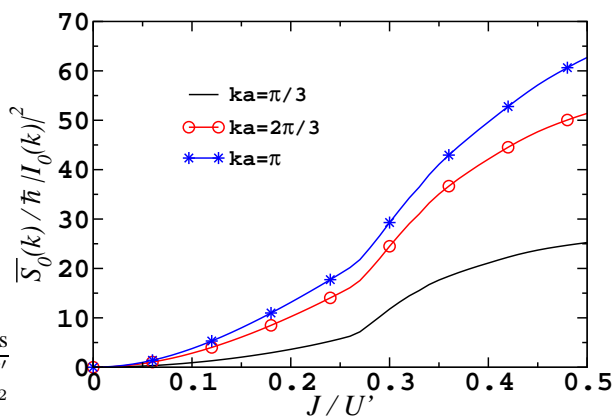


FIG. 13: (Color online) Static structure factor as a function of  $J$  in the hard-core limit at  $T = 0$  averaged over 200 disorder realizations.  $L = 200$ ,  $L' = 100$ ,  $N = 100$ .

repulsive interactions between the bosonic impurities and by Pauli's exclusion in the case of the fermionic ones. Since the impurities are assumed immobile, their statistics does not play any role. In fact, the interaction parameters  $U$  and  $U'$  can be tuned over a wider range by the additional use of Feshbach resonances.

To calculate the boundaries of the MI phases in the phase diagram for arbitrary lattice dimension  $d$  at zero temperature, we have applied the method of strong-coupling expansion. We have shown that the MI phase exists also for incommensurate bosonic fillings, and not only for commensurate ones. Furthermore, the binary disorder generates additional Mott lobes in the phase diagram.

For 1D lattices, we have investigated the superfluidity of soft-core bosons at  $T = 0$  for the binary disorder. Due to the exponential growth of the dimension of the bosonic Hilbert space for increasing boson numbers and numbers of lattice sites, exact numerical diagonalization is possible only for small lattices, which does not allow to control finite-size effects. However, the obtained results for small lattices are in good agreement with perturbative results obtained in Sec. III as well as with the exact results in the hard-core limit, see Sec. V A.

In the limit of infinitely strong repulsion (hard-core bosons), we have performed rather detailed exact studies by applying the Jordan-Wigner transformation. This allows to considerably reduce the computational complexity since all the properties of the strongly interacting system can be determined in terms of the solution of the single-particle problem. The remaining disorder average can straightforwardly be performed by standard numerical means. We have shown that the binary disorder destroys the superfluidity in the thermodynamic limit in a similar manner as for Gaussian disorder studied earlier. However, in contrast to the case of Gaussian or uniform disorder, we have found that the compressibility of the BG phase can be extremely low. Several experimentally measurable quantities such as the momentum distribution, the dynamical and static structure factors and the density of excited states have been worked out. The MI-BG transition can be identified via rather sharp kinks in the functional dependence of the maximum of the momentum distribution on the tunneling  $J$  (Fig. 10). Similar kinks occur in the static structure factor (Fig. 13). These kinks allow to identify the MI-BG quantum phase transition. The energy-dependence of the dynamical structure factor yields complementary information about the gap in the excitation spectrum in both phases (Fig. 12). Given the wide availability of elaborated experimental techniques, we hope that these predicted features will be found in real physical systems of ultracold atoms in the near future.

In the present work, we did not consider the effects of harmonic confinement which is normally present in most experiments with ultracold atoms in optical lattices. One can expect that our results will remain valid for shallow traps. On the other hand, coexistence of different phases in different spatial regions can come into play as in the case without disorder [5, 6] depending on the range of values of the local chemical potential in the region occupied by the atoms. For instance,

in the hard-core limit, there might be coexistence of the BG and MI with one boson per site, if  $J/U' > 0.25$ . In the opposite case  $J/U' < 0.25$ , MI with non-commensurate filling can coexist with the previous two phases. Detailed studies of the coexisting phases and experimental signatures of the corresponding QPT is a separate problem which requires further investigations.

## Acknowledgment

This work was supported by the SFB/TR 12 of the German Research Foundation (DFG).

- 
- [1] W. Zwerger, *Advances in Solid State Physics* **44**, 277 (2004).  
 [2] D. Jaksch and P. Zoller, *Ann. Phys. (NY)* **315**, 52 (2005).  
 [3] I. Bloch, *Nature Physics* **1**, 23 (2005).  
 [4] O. Morsch and M. Oberthaler, *Rev. Mod. Phys.* **78** 179 (2006).  
 [5] M. Lewenstein, A. Sanpera, V. Ahufinger, B. Damski, A. Sen(De), and U. Sen, *Advances in physics* **56**, 243 (2007).  
 [6] I. Bloch, J. Dalibard, W. Zwerger, *Rev. Mod. Phys.* (to be published), arXiv:0704.3011.  
 [7] J. E. Lye, L. Fallani, M. Modugno, D. S. Wiersma, and M. Inguscio, *Phys. Rev. Lett.* **95**, 070401 (2005).  
 [8] C. Fort, L. Fallani, V. Guarrera, J. E. Lye, M. Modugno, D. S. Wiersma, and M. Inguscio, *Phys. Rev. Lett.* **95**, 170410 (2005).  
 [9] D. Clément, A. F. Varón, M. Hugbart, J. A. Retter, P. Bouyer, L. Sanchez-Palencia, D. M. Gangardt, G. V. Shlyapnikov, and A. Aspect, *Phys. Rev. Lett.* **95**, 170409 (2005).  
 [10] T. Schulte, S. Drenkelforth, J. Kruse, W. Ertmer, J. Arlt, K. Sacha, J. Zakrzewski, and M. Lewenstein, *Phys. Rev. Lett.* **95**, 170411 (2005).  
 [11] H. Gimpferlein, S. Wessel, J. Schmiedmayer, and L. Santos, *Phys. Rev. Lett.* **95**, 170401 (2005); *Appl. Phys. B* **82**, 217 (2006).  
 [12] P. Kruger, *Phys. Rev. A* **76**, 063621 (2007); S. Wildermuth, S. Hofferberth, I. Lesanovsky, E. Haller, L. M. Andersson, S. Groth, I. Bar-Joseph, P. Kruger, J. Schmiedmayer, *Nature (London)* **435**, 440 (2005).  
 [13] P. Vignolo, Z. Akdeniz, and M. P. Tosi, *J. Phys. B* **36**, 4535 (2003).  
 [14] U. Gavish and Y. Castin, *Phys. Rev. Lett.* **95**, 020401 (2005).  
 [15] B. Horstmann, J. I. Cirac, and T. Roscilde, *Phys. Rev. A* **76**, 043625 (2007).  
 [16] B. Damski, J. Zakrzewski, L. Santos, P. Zoller, and M. Lewenstein, *Phys. Rev. Lett.* **91**, 080403 (2003).  
 [17] L. Sanchez-Palencia and L. Santos, *Phys. Rev. A* **72**, 053607 (2005).  
 [18] L. Fallani, J. E. Lye, V. Guarrera, C. Fort, and M. Inguscio, *Phys. Rev. Lett.* **98**, 130404 (2007).  
 [19] K. Byczuk, M. Ulmke, and D. Vollhardt, *Phys. Rev. Lett.* **90**, 196403 (2003); K. Byczuk, W. Hofstetter, and D. Vollhardt, *Phys. Rev. B* **69**, 045112 (2004); K. Byczuk and M. Ulmke, *Eur. Phys. J. B* **45**, 449 (2005); K. W. Kim, J. S. Lee, T. W. Noh, S. R. Lee, and K. Char, *Phys. Rev. B* **71**, 125104 (2005); N. Paris, A. Baldwin, and R. T. Scalettar, *Phys. Rev. B* **75**, 165113 (2007).  
 [20] A. Mering and M. Fleischhauer, *Phys. Rev. A* **77**, 023601 (2008).  
 [21] M. P. A. Fisher, P. B. Weichman, G. Grinstein, and D. S. Fisher, *Phys. Rev. B* **40**, 546 (1989).  
 [22] Similar treatment can be found in Ref. [20] where the analysis was restricted by  $d = 1$  and not all the possible values of the disorder parameter  $U'$  were explicitly considered.  
 [23] A. A. Abrikosov, L. P. Gor'kov and I. Ye. Dzyaloshinskii, *Quantum Field Theoretical Methods in Statistical Physics* (Pergamon Press, New York, 1965).  
 [24] K. V. Krutitsky, A. Pelster, and R. Graham, *New J. Phys.* **8**, 187 (2006).  
 [25] I. M. Lifshitz, *Sov. Phys. Usp.* **7**, 549 (1965) [*Usp. Fiz. Nauk* **83**, 617 (1964)]; F. Cyrot-Lackmann, *J. Phys. C* **5**, 300 (1972).  
 [26] J. K. Freericks and H. Monien, *Europhys. Lett.* **26**, 545 (1994); *Phys. Rev. B* **53**, 2691 (1996).  
 [27] R. Roth and K. Burnett, *Phys. Rev. A* **67**, 031602(R) (2003); *ibid.* **68**, 023604 (2003).  
 [28] M. E. Fisher, M. N. Barber, and D. Jasnow, *Phys. Rev. A* **8**, 1111 (1973); W. Krauth, *Phys. Rev. B* **44**, 9772 (1991).  
 [29] P. Jordan and E. Wigner, *Z. Phys.* **47**, 631 (1928).  
 [30] E. Lieb, T. Schultz, and D. Mattis, *Ann. Phys. (NY)* **16**, 407 (1961).  
 [31] A. De Martino, M. Thorwart, R. Egger, and R. Graham, *Phys. Rev. Lett.* **94**, 060402 (2005).  
 [32] T. Giamarchi and H. J. Schulz, *Europhys. Lett.* **3**, 1287 (1987); *Phys. Rev. B* **37**, 325 (1988).  
 [33] In the case of half-filling, this reproduces a well-known result  $f_s = 2/\pi$ . See, e.g., S. Rapsch, U. Schollwöck and W. Zwerger, *Europhys. Lett.* **46**, 559 (1999).  
 [34] V. A. Kashurnikov, N. V. Prokof'ev, and B. V. Svistunov, *Phys. Rev. A* **66**, 031601(R) (2002).  
 [35] T. Stöferle, H. Moritz, C. Schori, M. Köhl, and T. Esslinger, *Phys. Rev. Lett.* **92**, 130403 (2004).  
 [36] L. Pitaevskii and S. Stringari, *Bose-Einstein Condensation* (Clarendon Press, Oxford, 2003) and references therein.  
 [37] P. Vignolo and A. Minguzzi, *J. Phys. B* **34**, 4653 (2001).  
 [38] G. Pupillo, A. M. Rey, and G. G. Batrouni, *Phys. Rev. A* **74**, 013601 (2006).